Journal of the Mechanical Behavior of Biomedical Materials 89 (2019) 13–18

Contents lists available at ScienceDirect

Journal of the Mechanical Behavior of Biomedical Materials

journal homepage: www.elsevier.com/locate/jmbbm

The effect of pleural fluid layers on lung surface wave speed measurement: Experimental and numerical studies on a sponge lung phantom

Boran Zhou, Xiaoming Zhang*

Department of Radiology, Mayo Clinic College of Medicine and Science, 200 1st St SW, Rochester, MN 55905, USA

ARTICLE INFO

Keywords:
Lung ultrasound surface wave elastography (LUSWE)
Pleural effusion
Lung parenchyma
Lung sponge phantom
Finite element modeling (FEM)

ABSTRACT

Pleural effusion manifests as compression of pleural fluid on the lung parenchyma contributing to hypoxemia. Medical procedures such as drainage of plural fluid releases this compression and increases oxygenation. However, the effect of pleural effusion on the elasticity of lung parenchyma is unknown. By using lung ultrasound surface wave elastography (LUSWE) and finite element method (FEM), the effect of pleural effusion on the elasticity of superficial lung parenchyma in terms of surface wave speed measurement was evaluated in a sponge phantom study. Different thicknesses of ultrasound transmission gel used to simulated pleural fluid were inserted into a condom, which was placed between the sponge and standoff pad. A mechanical shaker was used to generate vibration on the sponge phantom at different frequencies ranging from 100 to 300 Hz while the ultrasound transducer was used to capture the motion for measurement of surface wave speed of the sponge. FEM was conducted based on the experimental setup and numerically assessed the influence of pleural effusion on the surface wave speed of the sponge. We found from FEM experiments that the influence of thickness of ultrasound transmission gel was statistically insignificant on the surface wave speed of the sponge at 100 and 150 Hz.

1. Introduction

Pleural effusion, frequently encountered in critically ill patients hospitalized in intensive care units (ICU), is the accumulation of excess fluid in the pleural cavity, which is the fluid-filled space that surrounds the lungs. It induces restrictive syndromes and increases the intrapulmonary shunt by compressing the lung parenchyma. Study has showed that pleural effusion may contribute to hypoxemia under mechanical ventilation (Balik et al., 2006). In order to increase oxygen delivery and oxygen consumption, medical procedures such as drainage of pleural fluid are performed to increase functional residual capacity and improve oxygenation. Hemodynamic and pulmonary parameters, such as blood pressure, systemic vascular resistance, peak airway pressure, were collected before and after the fluid was drained (Ahmed et al., 2004). However, no technique is able to evaluate the degree of restoration of the function of lung parenchyma.

In the ICU, the diagnosis of pleural effusion relies on the anteroposterior chest radiography obtained at bedside (Lichtenstein et al., 2004; Prim et al., 2016). However, it exposes patients to a high dose of radiation. Pleural sonography is an alternative imaging modality. It is a highly portable and widely accepted diagnostic technique for identifying pleural disease (Remérand et al., 2010; Mayo and Doelken, 2006; Twal et al., 2014). It permits imaging of pleural effusion and other pleural pathologies. In addition, ultrasonography is able to guide thoracentesis for pleural interventions. Normal visceral and parietal pleura are supposed and estimated at 0.2–0.3 mm thick. Pleural effusions with parietal pleural thickness > 10 mm, and diaphragmatic thickness > 7 mm predict underlying malignancy with high specificity. It has been shown that a minimum pleural effusion depth of 1.2 cm between the visceral and parietal pleura has been recommended to perform diagnostic thoracentesis (Soni et al., 2015; Shazly et al., 2015).

Thoracentesis is usually performed to relieve the compression of pleural effusion on the lung parenchyma. Few studies evaluated the restoration of lung parenchyma after drainage of pleural fluid. Function of lung parenchyma is heavily dependent on its elasticity. In order to noninvasively evaluate the elasticity of lung parenchyma for patients with interstitial lung disease (ILD), we recently developed a lung ultrasound surface wave elastography (LUSWE) to measure the surface wave speed of lung, which is correlated with lung elasticity (Zhang et al., 2017a, 2017b; Kalra et al., 2017; Clay et al., 2018). No pleural effusion was observed for ILD patients so ultrasound propagation can penetrate the thoracic muscle, and motion of lung surface can be captured by ultrasound imaging. For the patients with pleural effusion, the effect of pleural fluid on the surface wave speed of lung parenchyma in LUSWE is unknown. Therefore, there is a pressing need to develop a phantom model to systematically investigate the effect of pleural fluid

* Correspondence to: Department of Radiology, Mayo Clinic, 200 1st St SW, Rochester, MN 55905, USA.
E-mail address: Zhang.xiaoming@mayo.edu (X. Zhang).

https://doi.org/10.1016/j.jmbbm.2018.09.007
Received 14 May 2018; Received in revised form 3 August 2018; Accepted 5 September 2018
Available online 06 September 2018
1751-6161/

on the measurements of LUSWE.

Wet foam dressing material has been used for lung ultrasound simulation models to teach novice physicians to perform lung ultrasound in clinical situations (Lee et al., 2015). An economical sponge phantom was used for understanding and researching reverberation artifacts in lung ultrasound given its similar microstructure with lung parenchyma (Blüthgen et al., 2017). Moreover, with its availability, relevant phantom models for a systemic study of induced disease states, such as pulmonary edema, can be generated.

The objective of this study was to develop a phantom model for evaluating the effect of pleural fluid on surface wave speed in LUSWE. Ultrasound transmission gel to simulate pleural fluid was squeezed into a condom that was placed between the acoustic standoff pad and sponge phantom. In LUSWE, a shaker was used to generate a vibration on the surface of the standoff pad, and wave propagation on the surface of the sponge phantom was measured by using ultrasonic imaging and analysis. A FEM model was developed to simulate the wave propagation in the sponge phantom according to the experimental setup and compare with experimental measurements.

The rest of the paper is structured as follows: we describe the setup for the sponge phantom model in the Section 2; we present results that evaluate the effects of thickness of ultrasound transmission gel in the Section 3; we finalize the paper with Sections 4 and 5.

2. Materials and methods

2.1. Experimental setup

The experimental setting consisted of the following parts: (1) household sponge (Ocelo utility sponge, 3M, St. Paul, MN); (2) ultrasound transmission gel (Aquasonic 100, Parker Laboratories Inc, Fairfield, NJ); (3) an acoustic standoff pad (Aquaflex; Parker Laboratories Inc, Fairfield, NJ). The acoustic standoff pad is made of a gel matrix free of air bubbles eliminating the air-filled space between the transducer and the sponge phantom. Without a standoff pad, extrathoracic tissues will not be satisfactorily imaged. The fluid component of a pleural effusion may have echogenicity, which is characteristic of the presence of cellularity. Air bubbles within pleural fluid, which may occur with esophageal-pleural fistulas or a gas-forming infection will exhibit multiple mobile echogenic foci within pleural fluid that represent air bubbles (Cardenas-Garcia et al., 2015). Ultrasound transmission gel has a similar echogenicity as pleural fluid and can contain air bubbles in it. A sponge has been shown to have similar microstructure as lung parenchyma. Ultrasound transmission gel was squeezed into a condom that was placed between the standoff pad and sponge phantom. The condom was used to maintain the required thickness for the gel. The condom should not affect the acoustic properties of ultrasound transmission gel given its negligible weight and stiffness. The thickness of gel in the condom was measured using ultrasound imaging and also taking pictures with a ruler placed aside as reference. The thickness of ultrasound transmission gel was varied at 4 levels: 0 (base), 2 mm (level 1), 7 mm (level 2) and 12 mm (level 3). A sinusoidal vibration signal of 0.1 s duration was generated by a function generator (Model 33120A, Agilent, Santa Clara, CA). The vibration signals were used at five frequencies of 100, 150, 200, 250, and 300 Hz (Kubo et al., 2018a). The 100 Hz wave motion is stronger than the wave motion of higher frequency waves. The higher frequency waves have smaller wave length but decay rapidly over distance than the lower frequency waves. The frequency ranges chosen in this study consider the wave motion amplitude, spatial resolution, and wave attenuation. The excitation signal at a frequency was amplified by an audio amplifier (Model D150A, Crown Audio Inc., Elkhart, IN). This signal then drove an electromagnetic shaker (Model: FG-142, Labworks Inc., Costa Mesa, CA 92626) mounted on a stand. The shaker applied a 0.1 s harmonic vibration on the surface of the acoustic standoff pad using an indenter with 3 mm diameter. 0.1 s is selected to exclude most of the reflections from the data collection window while keeping the detected wave as a continuous wave. The propagation of the vibration wave in the sponge was measured using a linear array transducer (L11-5v, Philips Healthcare, Andover, MA) transmitting at default 6.4 MHz center frequency mounted on the acoustic standoff pad (Cheng et al., 2018). The transducer was connected to the ultrasound system (Vantage 1, Verasonics Inc., Kirkland, WA) (Fig. 1) (Zhang et al., 2018). The measurements were repeated three times at each frequency and each gel thickness.

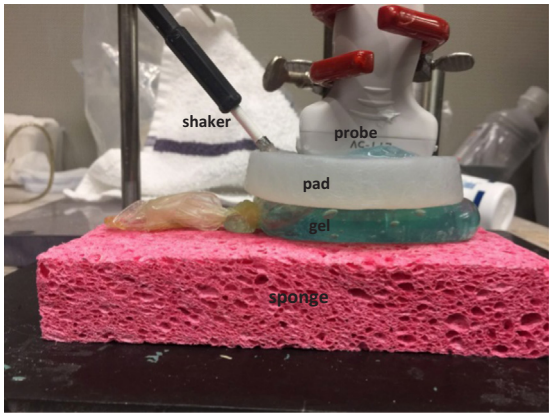

Fig. 1. Experimental setup of sponge phantom, transmission gel in a condom, and acoustic standoff pad.

2.2. Statistical analysis

An unpaired, two-tailed *t*-test of the differences in surface wave speed of the sponge phantom among different levels of gel thickness was conducted to compare sample means. Differences in mean values were considered significant at $p < 0.05$.

2.3. Numerical modeling

A FEM model was developed in ABAQUS (VERSION 6.14, 3DS Inc., Waltham, MA). The sponge phantom, acoustic standoff pad, and transmission gel in the condom were simulated as a 2D planar model of elastic medium (Fig. 2). Length and height of the acoustic standoff pad were 9 and 1.5 cm. Length and height of the sponge phantom were 12 and 2 cm. Ultrasound transmission gel thickness was predefined based on the measurements from experiments. The densities of the acoustic standoff pad and transmission gel were assumed to be 1000 kg m^{-3}. The structural constituent of the sponge phantom is cellulose, which has a density of 1500 kg m^{-3}. The sponge was modeled using a linear poroviscoelastic model assuming the void ratio of the sponge is 0.7. The standoff pad was assumed an incompressible, linear elastic material

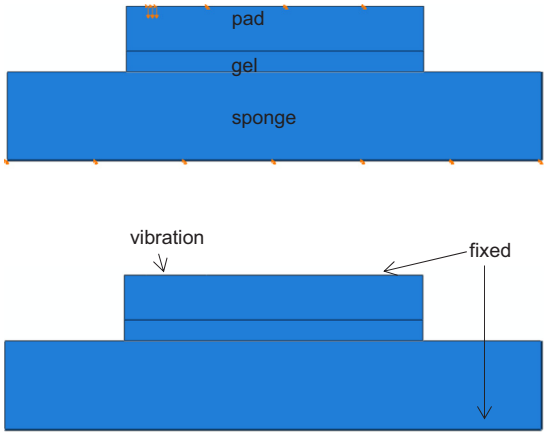

Fig. 2. Geometrical configuration of sponge phantom model.

(Chen et al., 2015). To the best of our knowledge, viscoelastic properties of the sponge phantom have not been quantified. The values of the material parameters of the sponge phantom were estimated based on the experimental measurements in terms of surface wave speed of the sponge phantom at different vibration frequencies. Given the Voigt model has widely been used for characterizing the dynamic behavior of soft biological tissues, Voigt model $\mu(t) = \mu_1 + \mu_2 \frac{\partial}{\partial t}$ is used in this study (Zhou and Zhang, 2018a). The surface wave speed using this model was calculated as:

$$c_s = \frac{1}{1.05}\sqrt{\frac{2(\mu_1^2 + \omega^2\mu_2^2)}{\rho(\mu_1 + \sqrt{\mu_1^2 + \omega^2\mu_2^2})}} \quad (1)$$

where c_s, ω, μ_1 and μ_2 are surface wave speed, angular frequency, shear elasticity, and shear viscosity, respectively. Given surface wave speeds of the sponge at five vibration frequencies, μ_1 and μ_2 were identified via least-square regression and used to calculate storage modulus G_s, loss modulus G_l, and long term modulus G_{inf},

$$G_s = \mu_1 \quad (2)$$

$$G_l = \omega\mu_2 \quad (3)$$

$$G_{inf} = \mu_1 \quad (4)$$

These quantities can then be implemented in ABAQUS in the frequency domain with frequency ranging from 100 to 300 Hz at an interval of 50 Hz (Table 1).

The model was excited using a segment source on the top left surface of standoff pad and the displacement was applied in the vertical direction (Fig. 2). Harmonic excitations were performed at 100, 150, 200, 250, and 300 Hz with duration of 0.1 s. The central segment of the acoustic standoff top surface pad and bottom surface of sponge were fixed in the horizontal and vertical directions. The bottom boundary of the sponge phantom was attached to an infinite region to minimize the wave reflections (Zhou et al., 2017; Zhou and Zhang, 2018b).

The mesh of sponge, standoff pad, and ultrasound transmission gel in the condom were constructed using linear quadrilateral plane stress elements (type CPS4R) with size 1 mm × 1 mm, enhanced with hourglass control and reduced integration, to minimize shear locking and hourglass effects. The infinite region was meshed by infinite elements (type CINPE4) with size 1 mm × 1 mm. The dynamic responses of the sponge phantom model to the excitations were solved by the ABAQUS implicit dynamic solver with automatic step size control. Mesh convergence tests were performed so that further refining the mesh did not change the solution significantly.

3. Results

Detection of sponge motion is guided by ultrasound imaging. Sponge motion at a given location can be analyzed by cross-correlation analysis of the ultrasound tracking beam. In this study, eight locations on the surface of the sponge phantom over a length of approximately 8 mm were selected to measure sponge motion (Fig. 3a). A high frame rate of 2000 frame/s is used to detect sponge motion in response to the vibration excitation at 100, 150, 200, 250, and 300 Hz. The surface wave speed is shown with 95% confidence interval, mean ± standard error (Fig. 3b). Fig. 6a shows the relationship between surface wave speed of the sponge phantom and gel thickness. Surface wave speed (SWS) of the sponge phantom increased with frequency at each level of gel thickness, from 3.28 ± 0.08 m/s at 100 Hz to 7.43 ± 0.19 m/s at 300 Hz. At the same frequency, no statistically significant difference in surface wave speed of the sponge phantom was seen at different levels of gel thickness.

Table 1
Material parameters of sponge phantom, acoustic standoff pad, and ultrasound transmission gel.

Materials	Sponge	Standoff pad	Transmission gel
E [kPa]		36.7	
v		0.499	
μ_1 **[kPa]**	6.83		1.3
μ_2 **[Pa s]**	24		24

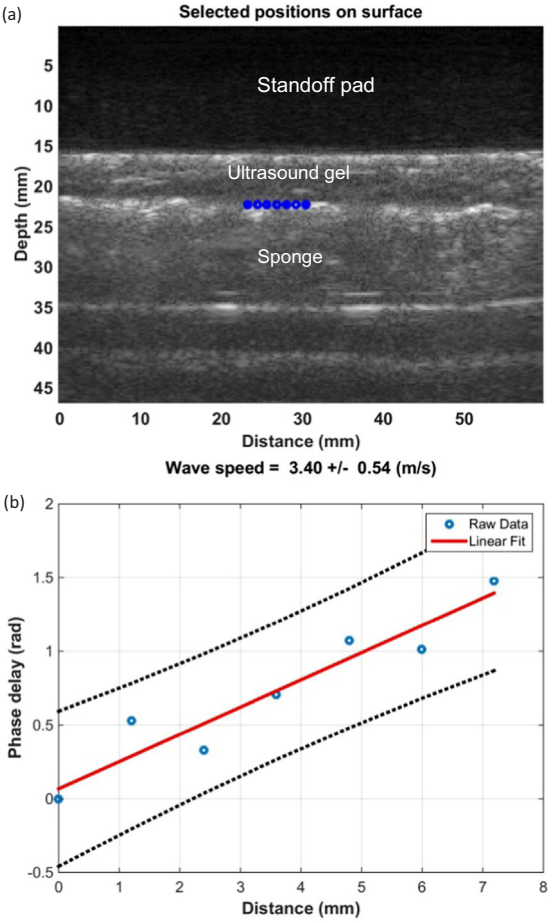

Fig. 3. (a) Representative B-mode image of sponge phantom model.

Eight locations on the surface of the sponge phantom were selected to measure the wave speed in the sponge by using the ultrasound tracking beam method. Blue dots indicate the points selected for measurement. Figure 3b is a representative phase delay-distance relationships of the sponge at frequency of 100 Hz. The wave phase change with position, in response to a 0.1 vibration was used to measure the wave speed.

FEM analysis of the sponge model was used to numerically investigate the effect of transmission of gel thickness on the surface wave speed of the sponge phantom. Results of the finite element simulations are summarized in Figs. 4–6. As the boundary of the sponge was assigned infinite elements, there is no wave reflection in the boundary (Fig. 4). The temporal-spatial displacement field of a central segment of sponge was extracted to minimize the influence of boundary effects. The phase velocity can be measured using 2D Fourier transform using the fast Fourier transform (FFT) on the spatiotemporal motion data. The resulting Fourier distribution, or k-space, has one temporal frequency (F) axis and one spatial frequency (K) axis. 2D-FFT of the displacement versus time data was performed using

$$U_y(K, F) = \sum_{m=}^{+\infty}{}_{-\infty} \sum_{n=-\infty}^{+\infty} u_y(x, t) e^{-j2\pi(Kmx+Fnt)} \quad (5)$$

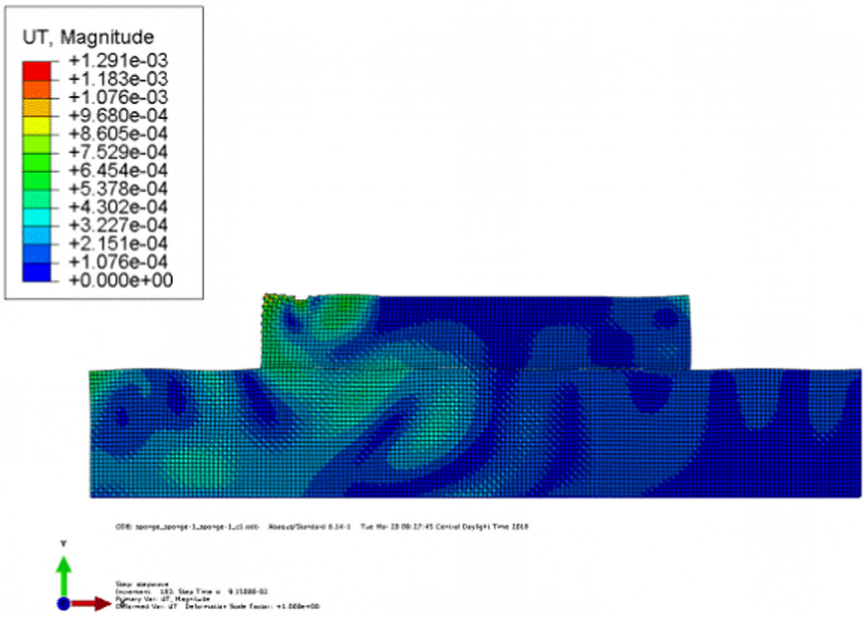

Fig. 4. Contour of translational displacement field of sponge phantom model due to harmonic vibration.

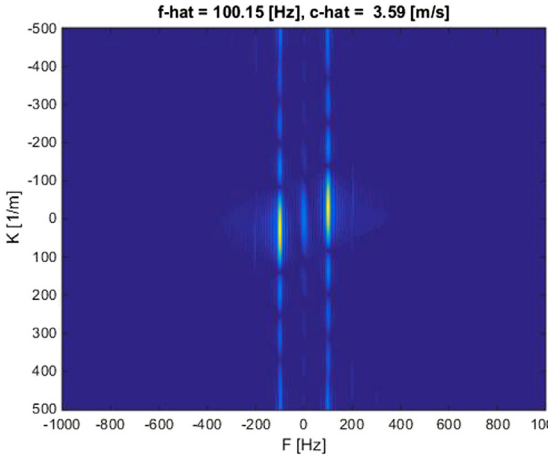

Fig. 5. Representative k-space from 2D FFT transformation of the sponge at 100 Hz excitation frequency.

where $u_y(x, t)$ is the motion of the sponge to the excitation as a function of distance from the excitation (x) and time (t). Here, K is the wave number and F is the temporal frequency of the wave. The coordinates of the k-space are the wave number (K) and the frequency (F) (Fig. 5) (Bernal et al., 2011; Kubo et al., 2018b). For the harmonic wave case, a peak will occur at the excitation frequency, and the coordinates where the peak occurs can be used to determine the phase velocity using

$$c_s = \frac{f_p}{k_p} \tag{6}$$

where c_s is the surface wave speed, $f_p$is the peak temporal frequency, and k_p is the peak spatial frequency.

The results from the numerical simulation showed that the surface wave speed (SWS) of the sponge phantom increased with excitation frequency at different levels of gel thickness (Fig. 6b). At 100 and 150 Hz, there was no significant difference in the surface wave speed of

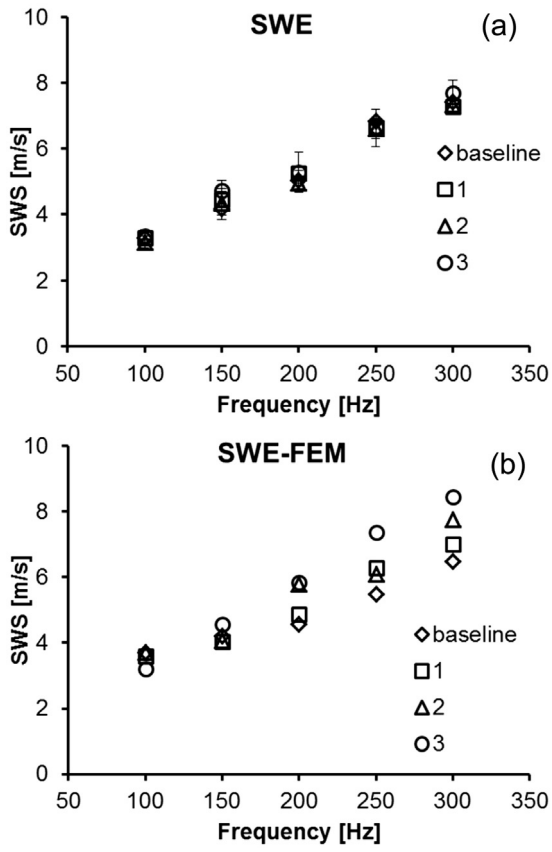

Fig. 6. (a) Surface wave speed (SWS)– gel thickness levels of sponge phantom at multiple frequencies (100, 150, 200, 250, and 300 Hz) from 3 repetitive measurements. Error bars represent the standard deviation of 3 repetitive measurements. (b) Surface wave speed (SWS)– gel thickness levels of sponge phantom at multiple frequencies (100, 150, 200, 250, and 300 Hz) from numerical simulations.

the sponge phantom at different levels of gel thickness. However, at 200, 250, and 300 Hz, there was increase in surface wave speed by 10% at ultrasound transmission gel thickness of 2 mm, 15% at 7 mm and 35% at 12 mm relative to the surface wave speed at base level of ultrasound gel thickness (Fig. 6b).

4. Discussions

The aim of this study was to develop a lung sponge phantom model to investigate the effect of pleural fluid on surface wave propagation in LUSWE. A sponge phantom, acoustic standoff pad, and ultrasound transmission gel were simulated as lung parenchyma, thoracic muscle, and pleural fluid. The level of transmission gel thickness was adjusted by squeezing different amounts of transmission gel into a condom that was placed between the acoustic standoff pad and sponge phantom. At each level of gel thickness, a shaker was used to generate a harmonic mechanical vibration on the acoustic standoff pad at frequencies of 100, 150, 200, 250 and 300 Hz. In our previous clinical study, we used a mechanical shaker to generate shear waves on the chest of patients and used the ultrasound transducer to capture the wave propagation of superficial lung parenchyma. In this study, we use the same experimental setup. The magnitude of the vibration is much lower than that of lung motion while the frequency (100–300 Hz) is higher than that of lung motion. The resulting wave propagation on the sponge surface was measured using an ultrasound transducer. A FEM model was developed according to the experimental setup to simulate the wave propagation on the surface of the sponge phantom. We found influence of ultrasound transmission gel thickness on the surface wave speed of the sponge insignificant at five different excitation frequencies from experiments. In FEM, at 100 and 150 Hz of excitation frequency, no significant influence of ultrasound transmission gel thickness on the surface wave speed of the sponge was observed; yet at 200, 250, and 300 Hz, the surface wave speed on the sponge increased with thickness of ultrasound transmission gel in FEM simulation.

The dynamic response of the sponge phantom obtained in our study has qualitatively similar trends with that of lung parenchyma in vivo, as both exhibit increasing shear wave speed with excitation frequency (Zhang et al., 2017a). The magnitude of surface wave speed of the sponge, which is an indicator of elasticity of the sponge, is higher than that of healthy subjects and similar with that of patients with interstitial lung disease (Zhang et al., 2017a; Kalra et al., 2017; Osborn et al., 2017). In our study, the surface wave speeds were at 3.2 ± 0.2 m/s 100 Hz, 4.35 ± 0.65 m/s at 150 Hz and 5.1 ± 0.78 m/s at 200 Hz. In our previous study for lung parenchyma of patients with interstitial lung disease, the surface wave speeds were 3.3 ± 0.37 m/s at 100 Hz, 4.38 ± 0.33 m/s at 150 Hz and 5.24 ± 0.44 m/s at 200 Hz (Zhang et al., 2017a). We are currently conducting LUSWE on sponge with injection of water to simulate pulmonary edema. Mass density of sponge should vary with different amounts of injected water, correspondingly altering the elasticity of sponge given the measured surface wave speed. The estimation of elasticity of lung tissue based on the wave speed is dependent on mass density of lung tissue. However, the data of mass density of lung is very limited, especially when the lung tissue is diseased or at various pulmonary pressures. We recently developed a deep neural network (DNN) model to predict lung mass density based on surface wave speeds obtained from lung ultrasound surface wave elastography (Zhou and Zhang, 2018c). In the future, we plan to use LUSWE and DNN to predict viscoelasticity of lung parenchyma. The presented model is of particular relevance to human models and this technique may be adapted to assess patients with pleural effusion.

Lung ultrasonography is more sensitive, specific, and reproducible for diagnosing lung pathologies and can be considered an alternative to bedside radiography and thoracic computed tomography (Lichtenstein et al., 2004). It can be used efficiently to evaluate the lung since more than 70% of the lung can be imaged through intercostal spaces (Mayo and Doelken, 2006). Lung ultrasonography is excellent for diagnosing pleural diseases, and it is especially useful in the emergency and critical care settings for the detection of pleural effusions or guidance of procedures such as thoracentesis (Mathis, 2003; Hakimisefat and Mayo, 2010). The volume of pleural fluid has been estimated via ultrasonography for mechanically ventilated patients or patients with thoracentesis (Balik et al., 2006; Vignon et al., 2005). Characterization of elasticity of superficial lung parenchyma is critically important for evaluating the function of lung parenchyma (Osborn et al., 2017; Zhang et al., 2017b). In LUSWE, the surface wave on the lung is safely generated by a local mechanical vibration on the chest. Diagnostic ultrasound is only used for detecting surface wave propagation on the lung. Hence, it is a noninvasive and safe technique for lung testing. With LUSWE, we plan to evaluate patients with pleural effusion via assessing elastic properties of superficial lung parenchyma prior and after drainage of pleural fluid.

Finite element modeling numerically evaluated the effects of ultrasound transmission gel on wave propagation of the sponge surface. FEM was used to validate the experimental results in this study. FEM offers flexibility for evaluating the complicated wave propagation in such a multi-layered material. Moreover, the boundary conditions can be adjusted to conduct a parametric study for evaluating the effects of pulmonary pressure on the elasticity of superficial lung parenchyma. In future, we plan to use the FEA for predicting the surface wave speed of superficial lung parenchyma at various pulmonary pressures. The infinite elements assigned on the boundary of muscle and lung were used to get rid of the wave reflection, and therefore, improve the accuracy of wave speed calculation. It showed that the wave speed increased with excitation frequency, which is in agreement with the obtained experimental measurements. The experimentally measured shear wave speeds at five excitation frequencies of the sponge surface were used to identify its viscoelasticity and the Voigt model was used. Different viscoelastic models may yield different results, and their predictions will be studied in a separate future work.

We hold that this investigation represents a meaningful contribution to the collective knowledge of LUSWE, but acknowledge that there are limitations to the study that merit further consideration. The ultrasound transmission gel used to simulate pleural fluid that occupies the pleural cavity is a gel-like substance. Given its mechanical behavior lies between Hookean solid and Newtonian fluid, the pleural fluid was modeled as a viscoelastic material with high viscosity. In the FEM, this viscoelastic material with high viscosity with different thickness may affect wave speed at different frequencies. Moreover, the sponge was assumed as a linear, poro-viscoelastic material with a void ratio of 0.7 given its similar structure with lung parenchyma (Luo et al., 2007). At higher frequencies, an increase in the surface wave speed of the sponge phantom at different levels of gel thickness could be due to a simplified assumption that the sponge phantom is a homogeneous material with void uniformly distributed in the sponge without air trapped within it. These approximations may cause discrepancy between FEM and LUSWE experimental results seen in the study. In the future, we plan to characterize the viscoelastic properties of ultrasound transmission gel using mechanical testing. Intercostal muscle was simulated using an acoustic standoff pad in this study. Structure and mechanical properties of intercostal muscle are more complicated than an acoustic standoff pad. The measured surface wave speed on the lung should have some contributions from the intercostal muscle. Lung sliding has been simulated using wet foam as lung parenchyma and hand as thoracic wall (Lee et al., 2015; Shokoohi and Boniface, 2012). Further improvement may use hand as thoracic wall or develop an ex-vivo animal model to investigate the effect of pleural fluid on the wave propagation of lung parenchyma in LUSWE.

5. Conclusion

In summary, the present manuscript develops a lung sponge

phantom model to integrate experimental measurements and numerical simulation to characterize the effect of pleural fluid on the dynamic response of the sponge phantom in terms of surface wave speed. Both the experiments and the FEM analyses showed that ultrasound transmission gel thickness has an insignificant effect on the surface wave speed of the sponge phantom at excitation frequencies of 100 and 150 Hz. The lung sponge phantom model may be useful for further developing ex vivo animal lung models and in vivo human lung studies.

Acknowledgements

This study is supported by NIH R01HL125234 from the National Heart, Lung and Blood Institute. We would like to thank Mrs. Jennifer Poston for editing this manuscript.

Conflict of interest

The authors declare that they have no conflict of interest.

References

Ahmed, S.H., et al., 2004. Hemodynamic and pulmonary changes after drainage of significant pleural effusions in critically Ill, mechanically ventilated surgical patients. J. Trauma Acute Care Surg. 57 (6), 1184–1188.
Balik, M., et al., 2006. Ultrasound estimation of volume of pleural fluid in mechanically ventilated patients. Intensive Care Med. 32 (2), 318.
Bernal, M., et al., 2011. Material property estimation for tubes and arteries using ultrasound radiation force and analysis of propagating modes. J. Acoust. Soc. Am. 129 (3), 1344–1354.
Blüthgen, C., et al., 2017. Economical sponge phantom for teaching, understanding, and researching A- and B-line reverberation artifacts in lung ultrasound. J. Ultrasound Med. 36 (10), 2133–2142.
Cardenas-Garcia, J., Mayo, P.H., Folch, E., 2015. Ultrasonographic evaluation of the pleura. Pleura 2 (2373997515610270).
Chen, L., et al., 2015. In vivo estimation of perineal body properties using ultrasound quasistatic elastography in nulliparous women. J. Biomech. 48 (9), 1575–1579.
Cheng, Y.-S., et al., 2018. Comparison of two ways of altering carpal tunnel pressure with ultrasound surface wave elastography. J. Biomech. 74, 197–201.
Clay, R., et al., 2018. Assessment of interstitial lung disease using lung ultrasound surface wave elastography: a novel technique with clinicoradiologic correlates. J. Thorac. Imaging.
Hakimisefat, B., Mayo, P.H., 2010. Lung ultrasonography. Open Crit. Care Med. J. 3 (2), 21–25.
Kalra, S., et al., 2017. Lung ultrasound surface elastography-preliminary measurements in patients with interstitial lung diseases. In: Respirology 22. Wiley, NJ, USA, pp. 90.
Kubo, K., et al., 2018a. The quantitative evaluation of the relationship between the forces applied to the palm and carpal tunnel pressure. J. Biomech. 66, 170–174.
Kubo, K., et al., 2018b. Ultrasound elastography for carpal tunnel pressure measurement: a cadaveric validation study. J. Orthop. Res. 36 (1), 477–483.
Lee, K.-H., et al., 2015. Evaluation of a novel simulation method of teaching B-lines: hand ultrasound with a wet foam dressing material. Clin. Exp. Emerg. Med. 2 (2), 89.
Lichtenstein, D., et al., 2004. Comparative diagnostic performances of auscultation, chest radiography, and lung ultrasonography in acute respiratory distress syndrome. Anesthesiol.: J. Am. Soc. Anesthesiol. 100 (1), 9–15.
Luo, H., Goldstein, I., Udelson, D., 2007. A three-dimensional theoretical model of the relationship between cavernosal expandability and percent cavernosal smooth muscle. J. Sex Med. 4 (3), 644–655.
Mathis, G., 2003B. Atlas of Chest Sonography. Springer Science & Business Media ISBN :3540442626, 9783540442622.
Mayo, P.H., Doelken, P., 2006. Pleural ultrasonography. Clin. Chest Med. 27 (2), 215–227.
Osborn, T., et al., 2017. A non-invasive ultrasound surface wave elastography technique for assessing interstitial lung disease. In: Arthritis & Rheumatology 69 WILEY, NJ, USA.
Prim, D.A., et al., 2016. A mechanical argument for the differential performance of coronary artery grafts. J. Mech. Behav. Biomed. Mater. 54, 93–105.
Remérand, F., et al., 2010. Multiplane ultrasound approach to quantify pleural effusion at the bedside. Intensive Care Med. 36 (4), 656–664.
Shazly, T., et al., 2015. On the Uniaxial Ring Test of Tissue Engineered Constructs. Exp. Mech. 55 (1), 41–51.
Shokoohi, H., Boniface, K., 2012. Hand ultrasound: a high-fidelity simulation of lung sliding. Acad. Emerg. Med. 19 (9).
Soni, N.J., et al., 2015. Ultrasound in the diagnosis & management of pleural effusions. J. Hosp. Med. 10 (12), 811–816.
Twal, W.O., et al., 2014. Cellularized Microcarriers as Adhesive Building Blocks for Fabrication of Tubular Tissue Constructs. Ann. Biomed. Eng. 42 (7), 1470–1481.
Vignon, P., et al., 2005. Quantitative assessment of pleural effusion in critically ill patients by means of ultrasonography. Crit. Care Med. 33 (8), 1757–1763.
Xiaoming Zhang, B.Z., Osborn, Thomas, Bartholmai, Brian, Greenleaf, James, Kalra, Sanjay, 2017a. Assessment of interstitial lung disease using lung ultrasound surface wave elastography. In: Proceedings of the Ultrasonics Symposium (IUS) 2017 IEEE International.
Xiaoming Zhang, B.Z., Kalra, Sanjay, Bartholmai, Brian, Greenleaf, James, Osborn, Thomas, 2017b. Quantitative assessment of scleroderma using ultrasound surface wave elastography. In: Proceedings of the Ultrasonics Symposium (IUS) 2017 IEEE International.
Zhang, X., et al., 2017a. Lung ultrasound surface wave elastography: a pilot clinical study. IEEE Trans. Ultrason. Ferroelectr. Freq. Control 64 (9), 1298–1304.
Zhang, X., et al., 2017b. An ultrasound surface wave elastography technique for non-invasive measurement of surface lung tissue. J. Acoust. Soc. Am. 141 (5) (3721-3721).
Zhang, X., et al., 2018. A novel noninvasive ultrasound vibro-elastography technique for assessing patients with erectile dysfunction and peyronie disease. Urology 116, 99–105.
Zhou, B., Zhang, X., 2018a. Comparison of five viscoelastic models for estimating viscoelastic parameters using ultrasound shear wave elastography. J. Mech. Behav. Biomed. Mater. 85, 109–116.
Zhou, B., Zhang, X., 2018b. Finite element analysis of lung ultrasound surface wave elastography. J. Acoust. Soc. Am. 143 (3) (1803-1803).
Zhou, B., Zhang, X., 2018c. Lung mass density analysis using deep neural network and lung ultrasound surface wave elastography. Ultrasonics 89, 173–177.
Zhou, B., Sit, A.J., Zhang, X., 2017. Noninvasive measurement of wave speed of porcine cornea in ex vivo porcine eyes for various intraocular pressures. Ultrasonics 81 (Suppl.C), S86–S92.